Irradiation of UVC LED at 277 nm inactivates coronaviruses by photodegradation of spike protein.

Authors: Qunxiang Ong[1]*, J. W. Ronnie Teo[2], Joshua Dela Cruz[1], Elijah Wee[1], Winson Wee[1], Weiping Han[1]*

Affiliations:

[1] Institute of Molecular and Cell Biology, Agency for Science, Technology and Research (A*STAR), 11 Biopolis Way, #02-02, Helios, Singapore, 138667, Singapore.

[2] Singapore Institute of Manufacturing Technology (SIMTech), Agency for Science, Technology and Research (A*STAR), 2 Fusionopolis Way, #08-04, Innovis, Singapore 138634, Singapore.

Corresponding author. Email: ongqx@imcb.a-star.edu.sg, wh10@cornell.edu

SUMMARY:

To interrupt SARS-CoV-2 transmission chains, Ultraviolet-C (UVC) irradiation has emerged as a potential disinfection tool to aid in blocking the spread of coronaviruses. While conventional 254-nm UVC mercury lamps have been used for disinfection purposes, other UVC wavelengths have emerged as attractive alternatives but a direct comparison of these tools is lacking with the inherent mechanistic properties unclear. Our results using human coronaviruses, hCoV-229E and hCoV-OC43, have indicated that 277-nm UVC LED is most effective in viral inactivation, followed by 222-nm far UVC and 254-nm UVC mercury lamp. While UVC mercury lamp is more effective in degrading viral genomic content compared to 277-nm UVC LED, the latter results in a pronounced photo-degradation of spike proteins which potentially contributed to the higher efficacy of coronavirus inactivation. Hence, inactivation of coronaviruses by 277-nm UVC LED irradiation constitutes a more promising method for disinfection.

INTRODUCTION

The novel coronavirus SARS-CoV-2 has precipitated into the COVID-19 pandemic, and at the time of writing, resulted in more than 171 million infections and 3 million deaths. The actual numbers should be much higher than reported, given the high incidence of asymptomatic cases escaping the capture by traditional diagnostic methods. Vaccination, masking, rigorous testing and thorough public disinfection strategies become vital prongs in combating virus spread within communities. Amongst the latter, ultraviolet irradiation presents as an attractive strategy, given its use being well established in inactivating viruses and killing other microbes(Lin et al., 2020; Raeiszadeh and Adeli, 2020). Consequently, UVC mercury lamps have been increasingly deployed in hospital settings.

UVC has been well known to possess germicidal properties and inactivate pathogenic microbes by damaging nucleic acids and proteins, thereby eliminating their ability to reproduce(Rauth, 1965; Sehgal, 1973; Setlow and Carrier, 1966; Werbin et al., 1966). The mechanism at which UV inactivates microbes depends highly on the specific wavelengths. 277nm UVC LEDs (Beck et al., 2017; Kim and Kang, 2018; Nguyen et al., 2019; Nunayon et al., 2020) and far UVC sources(Welch et al., 2018a, 2018b) have recently emerged as attractive alternatives to UVC mercury lamps. The former does not require mercury, which is banned by the Minamata Convention, has very short turn-on time, and is generally more reliable and has a longer lifetime(Song et al., 2016). The far UVC, on the other hand, is shown to be effective in inactivation of bacteria and human coronaviruses, and potentially poses less safety concerns for deployment(Barnard et al., 2020; Buonanno et al., 2020).

Numerous studies have studied the sensitivity of different microbes to UVC wavelengths, including human coronaviruses (Buonanno et al., 2020; Gerchman et al., 2020)and SARS-CoV-2(Inagaki et al., 2020; Kitagawa et al., 2020; Storm et al., 2020). However, no study to date has performed a direct comparative study on the efficacy of different UVC wavelengths on inactivation of coronaviruses. In addition, mechanistic insight into how different UVC wavelengths inactivate coronaviruses is severely lacking, and greater understanding in this area would facilitate their deployment in future pandemics. Here, we utilized human coronaviruses, HCoV-229E and OC43, for efficacy studies where 277nm UVC LED consistently

53 outperforms the other UVC wavelengths in inactivating coronaviruses. Mechanistic studies suggest that
54 this is achieved via a combination of photo-degradation of spike proteins and RNA molecules.
55

RESULTS

Utilizing human coronaviruses for UVC-induced inactivation studies

Coronaviruses are split into the four genera: Alphacoronavirus, Betacoronavirus, Gammacoronavirus and Deltacoronavirus(Fehr and Perlman, 2015; Woo et al., 2010). Among the different genera, alphacoronaviruses and betacoronaviruses have been known to infect mammals, and pose as a significant risk to the human population. The betacoronaviruses, MERS-CoV, SARS-CoV and SARS-CoV-2, may produce severe symptoms in patients while hCoV-OC43 and hCoV-229E cause about 15% of common colds (**Fig. 1A**). In terms of genomic organization, coronaviruses are the largest enveloped RNA viruses with positive single-stranded RNA molecules from 27 to 32 kilobases. The genome comprises of the replicase gene that encodes for the non-structural proteins of the genomes at about 20 kilobases, while similar structural proteins in the form of spike, envelop, membrane and nucleocapsid proteins are interspersed at the 3' end of the genome (**Fig. 1B**).

It has been established that RNA chains are directly disrupted by UVC by formation of pyrimidine dimers(Merriam and Gordon, 1967). The dimerization reaction occurs from adjacent pyrimidine bases in the form of uracil and cytosine(Beukers et al., 2010; Brown and Johns, 1968). We analyzed the genomic content of the coronaviruses based on these sequences as indicated their accession numbers from the NCBI Nucleotide: hCoV-OC43 (MW532119.1), hCoV-229e (KU291448.1) and SARS-CoV-2 (MW403500.1). We found that their overall base composition (**Fig. 1C**) and adjacent base arrangements (**Fig. 1D**) to be similar. We therefore hypothesize that the kinetics of UVC inactivation of hCoV-OC43 and hCoV-229E to be roughly similar.

Inactivation of human coronaviruses after exposure to different UVC wavelengths

To examine the inactivation efficacy of UVC on hCoV-OC43 and hCoV-229E, virus was placed on plastic petri dishes and expose to various UVC wavelengths of 73 μW/cm^2 for different timings ranging from 30 to 300 seconds (**Fig. S1-S2**). The reduction in infectivity of hCoV-OC43 (**Fig. 2A, Table S1**) and hCoV-229E (**Fig. 2B, Table S2**) can be observed after exposure to different UVC irradiation. The 277-nm UVC LED was most effective in carrying out the inactivation and achieved 3-log inactivation at 22 mJ/cm^2 for both human coronavirus strains, whereas 254-nm UV lamp achieved only 2-log inactivation for hCoV-OC43 and

1-log inactivation for hCoV-229E with the same dosage. Two-way ANOVA analyses of both sets of data reveal significant differences (**Table S1-2**) between the three UVC wavelengths in carrying out coronavirus inactivation ($p=0.0001$ and $p<0.0001$ for hCoV-OC43 and hCoV-229E respectively).

We next investigated the integration of hCoV-OC43 in human lung host cells after exposure to 300 seconds of UVC sources. **Fig. 2C** shows the representative images of human lung cells HCT-8 with hCoV-OC43 illuminated at different UVC wavelengths. We assessed the human cell lines for expression of the viral spike protein and found that 277-nm UVC outperforms the other UVC wavelengths in inactivation of coronaviruses.

Examining rates of nucleotide degradation under different UVC wavelengths.

To understand if the inactivation efficacy comes from RNA damage, we performed quantitative RT-PCR to examine the copy number of hCoV-OC43 after UVC irradiation. We observed that the copy number of hCoV-OC43 to be unperturbed after 300 seconds of 222-nm far UVC irradiation, while 254-nm UV lamp exerted the largest decrease in copy number followed by 277-nm UVC LED (**Fig. 3A**).

Photodegradation of hCoV-OC43 spike protein under 277-nm UVC LED

We next hypothesized that molecular components other than nucleic acids could be implicated, and the spike protein is an especially attractive target to pursue given that it facilitates viral transmission by binding to the host receptors(Shang et al., 2020). To this end, we subjected hCoV-OC43 to different duration of 254-nm and 277-nm UVC irradiation, and observed through western blot that the spike protein is degraded under 277-nm UVC LED and not under 254-nm UVC lamp. Silver staining of the viral lysate indicates the overall amount of protein loaded in each lane (**Fig. 3B**). To further confirm that spike protein is indeed degraded by 277-nm UVC LED, we performed UVC illumination on purified hCoV-OC43 spike proteins in vitro. Silver staining as depicted in **Fig. 3C** shows that hCoV-OC43 spike protein presents at a lower intensity under 277-nm UVC LED and not under 254-nm UV lamp. This is further corroborated by absorbance spectroscopy in **Fig. 3C** which demonstrates a shift in absorbance upon 277-nm UVC LED illumination but not 254-nm UV lamp.

Photodegradation of SARS-CoV-2 spike protein under 277-nm UVC LED

First, we exposed SARS-CoV-2 spike protein S1 subunit to varied durations of 254-nm UVC lamp and 277-nm UVC LED and observed the reduction of the full-length spike protein band under 277-nm UVC LED and not under 254-nm UVC LED. This happens on both glycosylated and non-glycosylated forms of the spike protein (**Fig. 4A**). Absorbance spectroscopy (**Fig. 4B**) analysis showed the UV absorbance profile of 254-nm lit proteins to be relatively unchanged while there is an increase of absorbance profile in the 250-300 nm region for 277-nm lit proteins. Western blot (**Fig. 4C**) analysis further revealed a reduction in the SARS-CoV-2 spike S1 proteins under low loading of protein samples, but under higher loadings, aggregates of spike protein in the form of dimers and trimers could be seen in a dose-dependent manner.

In the search for potential mechanisms that drive the absorption of 277-nm wavelengths and degradation / aggregation of the proteins, we studied the structure of the SARS-CoV-2 S glycoprotein (PDB: 6VXX) (Walls et al., 2020) and looked for aromatic amino acids in proximity to disulfide bonds as possible active regions upon 277-nm UVC irradiation. In particular, tryptophan has high molar absorptivity at the 280-nm wavelength and has been known to mediate energy transfer and neighboring disulfide bond breakage (Beaven and Holiday, 1952; Chan et al., 2006; Kerwin and Remmele, 2007; Wu et al., 2008). We identified the Trp 436 as a key antenna of 277-nm absorption, and conducted studies on W436R receptor binding domain (RBD) mutant alongside wild type, F377L and Y453F mutants, that are in close proximity but unlinked to the W436-C336-C361 transfer chain (**Fig. 4D**). We illuminated the RBD samples with 0, 2, 5, 10 minutes of 277-nm UVC LED and studied the rate of oligomerization for each sample by probing with SARS-CoV-2 Spike antibody (**Fig. 4E**). It is observed that W436R mutant has a lower rate of aggregation compared to the other species and this is quantified by comparing the intensity of the monomer fraction (at 35kDa) with respect to the rest of the lane for samples illuminated with 5 minutes of 277-nm UVC LED (**Fig. 4F**). Absorbance spectroscopy further verified that after 10 minutes of UVC LED illumination, the W436R mutant did not exhibit as significant changes in absorbance compared to the wild-type and Y453F mutant.

DISCUSSION

In this study, we focused on human coronaviruses hCoV-OC43 and hCoV-229E, which belong to the genus beta-coronavirus and alpha-coronavirus respectively. In particular, hCoV-OC43 could be considered as a surrogate for SARS-CoV-2 and the conclusions drawn here on UVC efficacy can thus be extrapolated to SARS-CoV-2. On the other hand, hCoV-229E resembles the viruses that causes the common cold. The viral efficacy tests performed here not only targeted the current COVID-19 pandemic, but also applies to future coronaviral pandemics in general.

While many studies have individually tested the 222-nm far UVC lamp, 254-nm UVC lamp and broad ranges of UVC LEDs for their efficacy towards viruses, this is the first study to report the mechanisms through which viral inactivation occurs. In summary, we find that 277-nm UVC LED outperforms the other UVC wavelengths in inactivation of human coronaviruses, and this could be aided by the contribution from spike protein degradation with absorption of UV wavelengths at Trp 436. We also find that 222-nm UVC LED does not affect the genomic material of beta-coronavirus, an observation that is congruent with a previous report (Kitagawa et al, 2020).

It has been widely believed that the efficacy of UV germicidal irradiation (UVGI) is dependent largely on the absorption by the target nucleic acids. While the mechanism holds significant merit, it is important to examine the other molecular mechanisms at which UV tools could exert their germicidal properties. It is thus important to consider the viral components individually as we characterize the multitude of UVGI solutions available to combat the current and future pandemics.

LIMITATIONS OF STUDY

Due to the lack of access to BSL-3 facilities, we were unable to perform the viral infectivity tests on SARS-CoV-2 or the relevant variants. However, this limitation is mitigated by our studies on the beta coronavirus hCoV-OC43, which provides a close approximation towards SARS-CoV-2 with the relevant structures of the spike proteins being relatively similar.

158 **Figures**

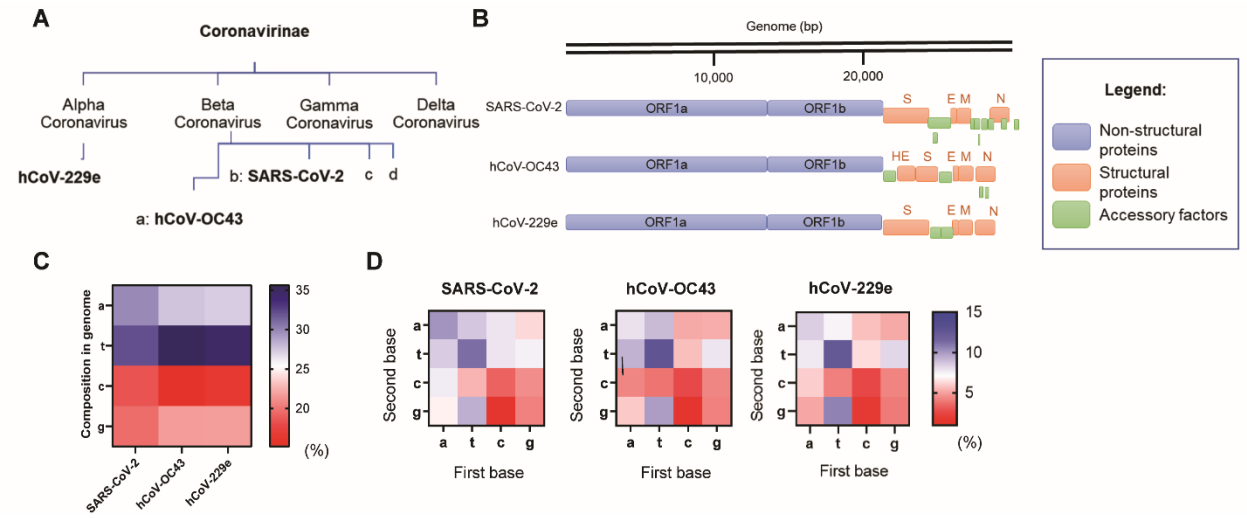

159

160 **Figure 1. Utilizing human coronaviruses for UVC-induced inactivation studies**

161 (a) The different genera of the coronavirus family. Alpha and beta-coronaviruses with the various
162 highlighted viruses, hCoV-229e, hCoV-OC43 and SARS-CoV-2.

163 (b) Genome organizations of SARS-CoV-2, hCoV-OC43 and hCoV-229e.

164 (c) Overall base composition of SARS-CoV-2, hCoV-OC43 and hCoV-229e.

165 (d) Adjacent base composition of SARS-CoV-2, hCoV-OC43 and hCoV-229e.

166

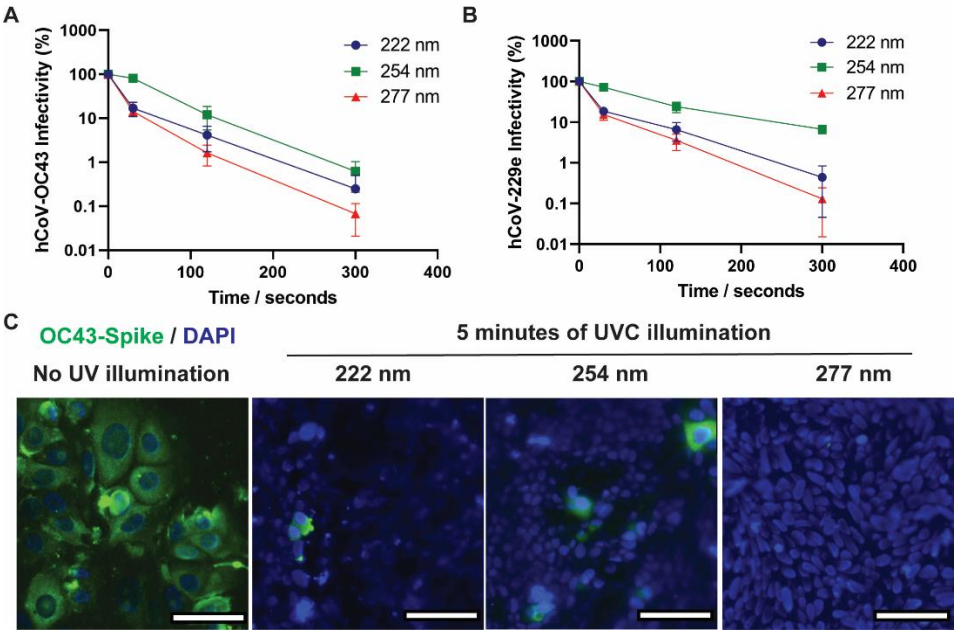

Figure 2. Inactivation of human coronaviruses after exposure to different UVC wavelengths

(a) HCoV-OC43 infectivity as a function of the duration of different UVC sources at 73 µW/cm^2. Infectivity is defined as a function of PFU_{UV}/PFU_{NoUV}. Values are reported as mean +/- SD from n = 3 experiments.

(b) HCoV-229e infectivity as a function of the duration of different UVC sources at 73 µW/cm^2. Infectivity is defined as a function of PFU_{UV}/PFU_{NoUV}. Values are reported as mean +/- SD from n=3 experiments.

(c) Infection of human lung cell line, HCT-8 from irradiated and untreated hCoV-OC43. Green fluorescence indicates infected cells while blue fluorescence indicates DAPI stains of nuclei. Images were acquired with a 40x objective, with the scale bars at 50 µm.

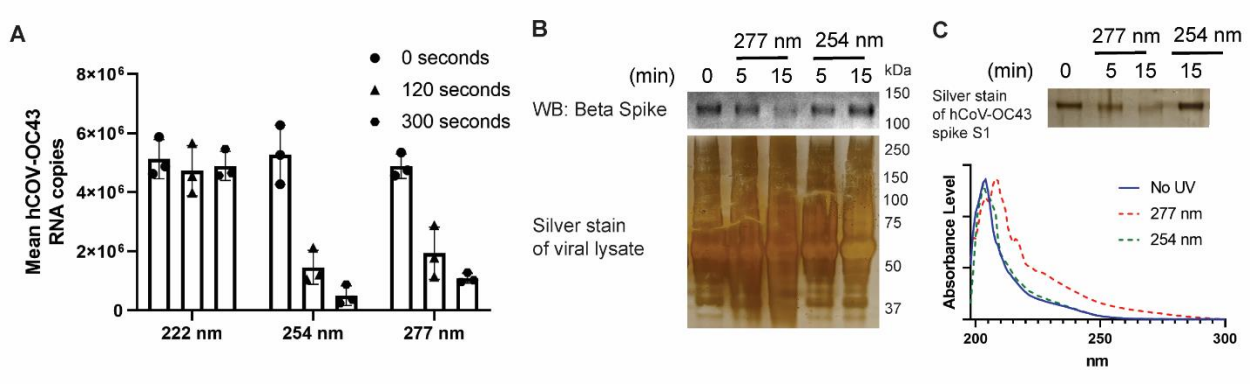

Figure 3. 277nm UVC LED's higher efficacy at inactivation of coronavirus is not due to UV-induced genomic damage and could be due to spike protein degradation.

(a) Quantitative RT-PCR reveals that the copy number of hCoV-OC43 did not change due to 222-nm illumination, and decrease the fastest due to 254-nm UVC lamp. Values are reported as mean +/- SD from n=3 experiments.

(b) Beta spike glycoprotein of hCoV-OC43 is found to diminish in intensity upon 15 minutes of 277-nm UVC LED illumination but not under 254-nm UVC lamp. Silver stain of viral lysate is provided to show the total loading on each lane.

(c) Purified hCoV-OC43 spike S1 proteins is found to diminish in intensity upon 15 minutes of 277-nm UVC LED illumination but not under 254-nm UVC lamp. Changes in absorbance spectra of hCoV-OC43 spike S1 observed after 15 minutes of 277-nm UVC LED irradiation but not 254-nm UVC lamp.

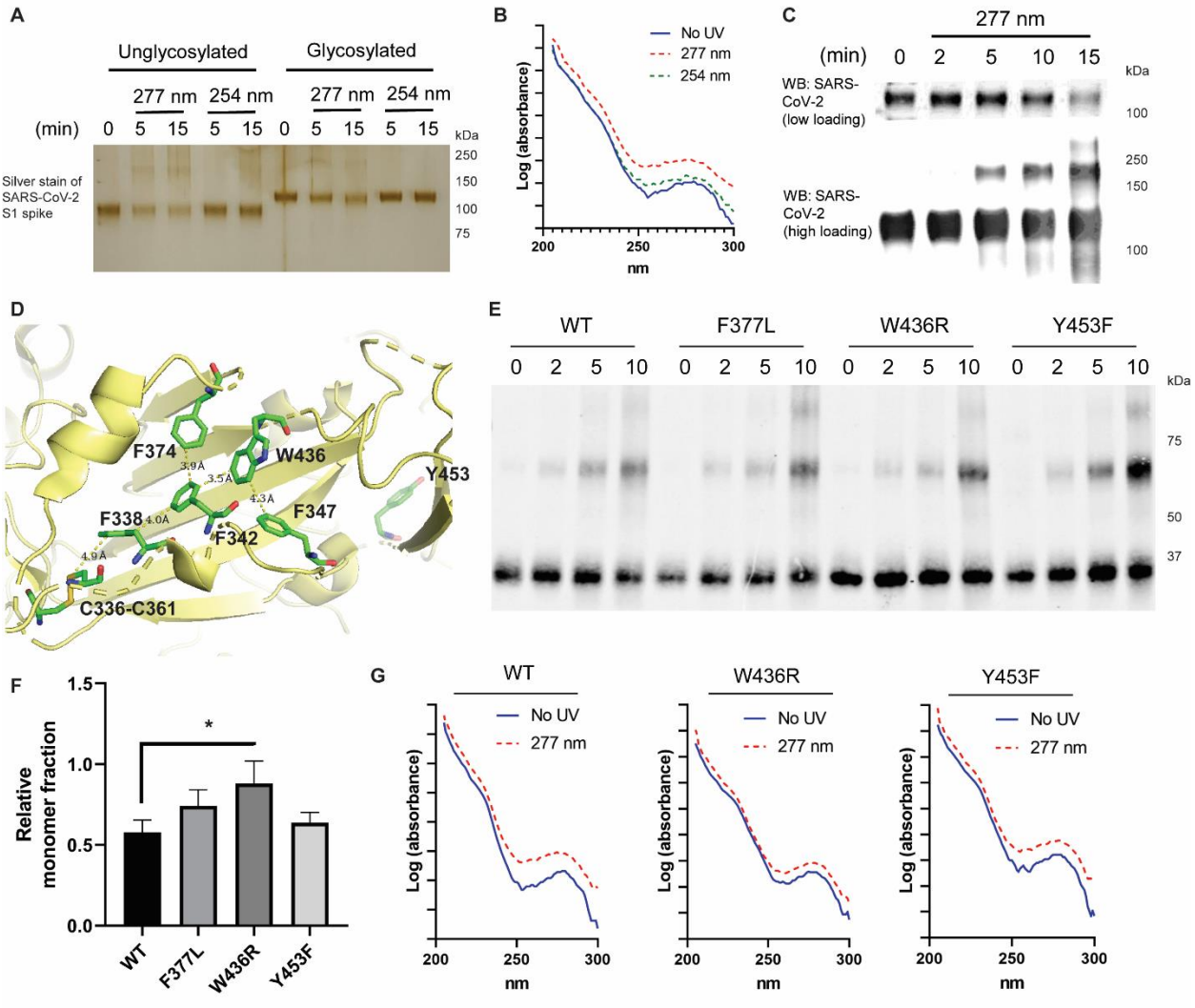

Figure 4. Photodegradation of SARS-CoV-2 spike protein under 277nm UVC LED

(a) Silver stains of un-glycosylated and glycosylated SARS-CoV-2 spike S1 protein under different UVC treatment.

(b) Changes in absorbance spectra of SARS-CoV-2 spike S1 observed after 15 minutes of 277-nm UVC LED irradiation but not 254-nm UVC lamp.

(c) Western blot analysis of SARS-CoV-2 spike S1 protein revealed that while the protein level of SARS-CoV-2 decreases under 277-nm UVC LED, higher aggregates could be observed upon higher UVC dose.

(d) SARS-CoV2 spike protein structure (PDB: 6VXX). Key residues centered around W436 that could potentially act as an antenna for 277nm UVC absorption. Y453 is depicted in the background while F377 is adjacent to F374 (not highlighted in the schematic).

(e) Western blot analysis of SARS-CoV-2 spike S1 RBD proteins revealed the differential rate of aggregation and degradation amongst the different mutants.

(f) Quantification of relative monomer fraction for wild type and mutant RBD proteins. The fraction is calculated as a function of (intensity at 35kDa) / (overall intensity across the whole lane).

(g) Absorbance spectra of the RBD proteins reveal little changes in 250-300 nm UVC absorbance for W436R compared to wild type and Y453F mutant, indicating potentially that W436R spike protein is less susceptible to 277nm UVC LED treatment.

ASSOCIATED CONTENT

Supporting Information. The following files are available free of charge.

Figure S1. Wavelength spectrum of different UVC light sources

Figure S2. Schematic diagram of UVC enclosure

Table S1. Two-way ANOVA results for hCoV-OC43 infectivity curves

Table S2. Two-way ANOVA results for hCoV-229e infectivity curves

Author Contributions

The manuscript was written through contributions of all authors. Here entails the list of contributions made by each author:- Conceptualization: QO, JWRT, WH; Methodology: QO, JWRT; Investigation: QO, JWRT, JDC, EW, WW; Funding acquisition: QO, JWRT; Writing – original draft: QO, WH; Writing – review & editing: JWRT, JDC, EW, WW. All authors have given approval to the final version of the manuscript.

Funding Sources

We would like to thank our funding sources:- National Research Foundation grant NRF2020NRF-CG002-035 (awarded to QO, JWRT) and Accelerate Technologies Gap-funded project GAP/2020/00392 (awarded to JWRT, QO).

ACKNOWLEDGMENT

We thank Dr. Edward George Robins, Dr. Yaw-Sing Tan, Dr. Janarthanan Krishnamoorthy and Ms. Haitong Mao for proofreading of the manuscript; we thank Prof. Lisa Ng, Prof. Xianjun Loh, Dr. Yuanjie Liu, Ms. Siew Lan Lim and Dr. Sun-Yee Kim for providing technical advice and help.

REFERENCES

Barnard, I.R.M., Eadie, E., and Wood, K. (2020). Further evidence that far-UVC for disinfection is unlikely to cause erythema or pre-mutagenic DNA lesions in skin. Photodermatol. Photoimmunol. Photomed. *36*, 476–477.

Beaven, G.H., and Holiday, E.R. (1952). Ultraviolet Absorption Spectra of Proteins and Amino Acids. Adv. Protein Chem. *7*, 319–386.

239 Beck, S.E., Ryu, H., Boczek, L.A., Cashdollar, J.L., Jeanis, K.M., Rosenblum, J.S., Lawal, O.R., and Linden,
240 K.G. (2017). Evaluating UV-C LED disinfection performance and investigating potential dual-wavelength
241 synergy. Water Res. *109*, 207–216.

242 Beukers, R., Ylstra, J., and Berends, W. (2010). The effect of ultraviolet light on some components of the
243 nucleic acids: II: In rapidly frozen solutions. Recl. Des Trav. Chim. Des Pays-Bas *77*, 729–732.

244 Brown, I.H., and Johns, H.E. (1968). PHOTOCHEMISTRY OF URACIL. INTERSYSTEM CROSSING AND
245 DIMERIZATION IN AQUEOUS SOLUTION. Photochem. Photobiol. *8*, 273–286.

246 Buonanno, M., Welch, D., Shuryak, I., and Brenner, D.J. (2020). Far-UVC light (222 nm) efficiently and
247 safely inactivates airborne human coronaviruses. Sci. Rep. *10*, 1–8.

248 Chan, H.-L., Gaffney, P.R., Waterfield, M.D., Anderle, H., Peter Matthiessen, H., Schwarz, H.-P., Turecek,
249 P.L., and Timms, J.F. (2006). Proteomic analysis of UVC irradiation-induced damage of plasma proteins:
250 Serum amyloid P component as a major target of photolysis. FEBS Lett. *580*, 3229–3236.

251 Fehr, A.R., and Perlman, S. (2015). Coronaviruses: An overview of their replication and pathogenesis. In
252 Coronaviruses: Methods and Protocols, (Springer New York), pp. 1–23.

253 Gerchman, Y., Mamane, H., Friedman, N., and Mandelboim, M. (2020). UV-LED disinfection of
254 Coronavirus: Wavelength effect. J. Photochem. Photobiol. B Biol. *212*, 112044.

255 Inagaki, H., Saito, A., Sugiyama, H., Okabayashi, T., and Fujimoto, S. (2020). Rapid inactivation of SARS-
256 CoV-2 with deep-UV LED irradiation. Emerg. Microbes Infect. *9*, 1744–1747.

257 Kerwin, B.A., and Remmele, R.L. (2007). Protect from light: Photodegradation and protein biologics. J.
258 Pharm. Sci. *96*, 1468–1479.

259 Kim, D.K., and Kang, D.H. (2018). UVC LED irradiation effectively inactivates aerosolized viruses, bacteria,
260 and fungi in a chamber-type air disinfection system. Appl. Environ. Microbiol. *84*.

261 Kitagawa, H., Nomura, T., Nazmul, T., Omori, K., Shigemoto, N., Sakaguchi, T., and Ohge, H. (2020).
262 Effectiveness of 222-nm ultraviolet light on disinfecting SARS-CoV-2 surface contamination. Am. J. Infect.
263 Control *49*, 299–301.

264 Lin, Q., Lim, J.Y.C., Xue, K., Yew, P.Y.M., Owh, C., Chee, P.L., and Loh, X.J. (2020). Sanitizing agents for
265 virus inactivation and disinfection. View *1*.

266 Merriam, V., and Gordon, M.P. (1967). PYRIMIDINE DIMER FORMATION IN ULTRAVIOLET
267 IRRADIATED TMV-RNA. Photochem. Photobiol. *6*, 309–319.

268 Nguyen, T.M.H., Suwan, P., Koottatep, T., and Beck, S.E. (2019). Application of a novel, continuous-

feeding ultraviolet light emitting diode (UV-LED) system to disinfect domestic wastewater for discharge or agricultural reuse. Water Res. *153*, 53–62.

Nunayon, S.S., Zhang, H., and Lai, A.C.K. (2020). Comparison of disinfection performance of UVC-LED and conventional upper-room UVGI systems. Indoor Air *30*, 180–191.

Raeiszadeh, M., and Adeli, B. (2020). A Critical Review on Ultraviolet Disinfection Systems against COVID-19 Outbreak: Applicability, Validation, and Safety Considerations. ACS Photonics *7*, 2941–2951.

Rauth, A.M. (1965). The Physical State of Viral Nucleic Acid and the Sensitivity of Viruses to Ultraviolet Light. Biophys. J. *5*, 257–273.

Sehgal, O.P. (1973). Inactivation of southern bean mosaic virus and its ribonucleic acid by nitrous acid and ultraviolet light. J. Gen. Virol. *18*, 1–10.

Setlow, R.B., and Carrier, W.L. (1966). Pyrimidine dimers in ultraviolet-irradiated DNA's. J. Mol. Biol. *17*, 237–254.

Shang, J., Wan, Y., Luo, C., Ye, G., Geng, Q., Auerbach, A., and Li, F. (2020). Cell entry mechanisms of SARS-CoV-2. Proc. Natl. Acad. Sci. U. S. A. *117*, 11727–11734.

Song, K., Mohseni, M., and Taghipour, F. (2016). Application of ultraviolet light-emitting diodes (UV-LEDs) for water disinfection: A review. Water Res. *94*, 341–349.

Storm, N., McKay, L.G.A., Downs, S.N., Johnson, R.I., Birru, D., de Samber, M., Willaert, W., Cennini, G., and Griffiths, A. (2020). Rapid and complete inactivation of SARS-CoV-2 by ultraviolet-C irradiation. Sci. Rep. *10*, 1–5.

Vijgen, L., Keyaerts, E., Moës, E., Maes, P., Duson, G., and Van Ranst, M. (2005). Development of one-step, real-time, quantitative reverse transcriptase PCR assays for absolute quantitation of human coronaviruses OC43 and 229E. J. Clin. Microbiol. *43*, 5452–5456.

Walls, A.C., Park, Y.J., Tortorici, M.A., Wall, A., McGuire, A.T., and Veesler, D. (2020). Structure, Function, and Antigenicity of the SARS-CoV-2 Spike Glycoprotein. Cell *181*, 281–292.e6.

Welch, D., Buonanno, M., Grilj, V., Shuryak, I., Crickmore, C., Bigelow, A.W., Randers-Pehrson, G., Johnson, G.W., and Brenner, D.J. (2018a). Far-UVC light: A new tool to control the spread of airborne-mediated microbial diseases. Sci. Rep. *8*, 2752.

Welch, D., Spotnitz, H.M., Brenner, D.J., Randers-Pehrson, G., Buonanno, M., and Shuryak, I. (2018b). Far-UVC light applications: sterilization of MRSA on a surface and inactivation of aerosolized influenza virus. In Light-Based Diagnosis and Treatment of Infectious Diseases, T. Dai, ed. (SPIE), p. 60.

299 Werbin, H., Hidalgo-Salvatierra, O., Seear, J., and McLaren, A.D. (1966). Comparative photoreactivation
300 of ultraviolet light-inactivated tobacco mosaic virus ribonucleic acid on Chenopodium, pinto bean, and
301 tobacco plants. Virology *28*, 202–207.

302 Woo, P.C.Y., Huang, Y., Lau, S.K.P., and Yuen, K.-Y. (2010). Coronavirus Genomics and Bioinformatics
303 Analysis. Viruses *2*, 1804–1820.

304 Wu, L.Z., Sheng, Y.B., Xie, J. Bin, and Wang, W. (2008). Photoexcitation of tryptophan groups induced
305 reduction of disulfide bonds in hen egg white lysozyme. J. Mol. Struct. *882*, 101–106.

306 Photochemistry and Photobiology of Nucleic Acids - 1st Edition.

307

MATERIALS AND METHODS

KEY RESOURCES TABLE

REAGENT or RESOURCE	SOURCE	IDENTIFIER
Antibodies		
Anti-Coronavirus OC43 Spike Protein antibody	Cusabio	CSB-PA336163EA01HIY
SARS-CoV-2 Spike RBD antibody	Sinobiological	40592-T62
Bacterial and virus strains		
HCoV-229E	ATCC	VR-740
HCoV-OC43	ATCC	VR-1588
Chemicals, peptides, and recombinant proteins		
EMEM	ATCC	30-2003
RPMI-1640	ATCC	30-2011
Purified recombinant spike proteins	Sinobiological	40592-V08H80, 40591-V08H3, 40592-V08H9, 40592-V08H27, 40591-V08H, 40607-V08H1
Carboxymethylcellulose	Sigma Aldrich	C4888
Critical commercial assays		
QiAmp Viral RNA mini kit	Qiagen	
TaqPath 1-step RT-qPCR master mix CG	Applied Biosystems	
Pierce™ Silver Stain Kit	Thermofisher	
Deposited data		
SARS-CoV-2 Spike Protein	PDB	6VXX
hCoV-OC43	NCBI Nucleotide database	MW532119.1
hCoV-229e	NCBI Nucleotide database	KU291448.1
SARS-CoV-2	NCBI Nucleotide database	MW403500.1
Experimental models: Cell lines		
MRC-5	ATCC	CCL-171
HCT-8	ATCC	CCL-244
Oligonucleotides		
Forward Primer for qRT-PCR of HCoV-OC43: 5'-ATGTTAGGCCGATAATTGAGGACTAT-3	Vjigen et al	
Reverse Primer for qRT-PCR of HCoV-OC43: 5′-AATGTAAAGATGGCCGCGTATT-3′	Vjigen et al	
Software and algorithms		
ImageJ	Schneider et al., 2012	https://imagej.nih.gov/ij/
GraphPad Prism Sotware 8.4.3	GraphPad Inc.	
Quantstudio 5 software	Applied Biosystems	
Other		
222-nm far UVC lamp	Ushio	N.A.
254-nm UVC mercury lamp	Sankyo Denki	G8T5

277-nm UVC LED	Lextar	PU35CM1
Spectroradiometer	GL Optic	GL Spectis 4.0

310

311 Viral strains and viral propagation

312 HCoV-229E (ATCC VR-740) and hCoV-OC43 (ATCC VR-1558) were propagated in human lung fibroblasts
313 MRC-5 (ATCC CCL-171) and colon adenocarcinoma cells HCT-8 (ATCC CCL-244) respectively (all from
314 ATCC, Manassas, VA). The MRC-5 fibroblasts were grown in EMEM (ATCC 30-2003) supplemented with
315 10% Fetal Bovine Serum (FBS), 100 U/ml penicillin and 100 µg/ml streptomycin (Sigma-Aldrich, St. Louis,
316 MO). The HCT-8 epithelial cells were cultured in RPMI-1640 supplemented with 10% horse serum, 100
317 U/ml penicillin and 100 µg/ml streptomycin. The virus infection medium is made up of EMEM or RPMI-1640
318 with 2% FBS or horse serum for hCoV-229E and hCoV-OC43 respectively.

319 UV sources and irradiance measurement

320 To understand the effect of UVC wavelength on human coronaviruses, three different UVC light sources –
321 222-nm far UVC lamp (Ushio), 254-nm UVC mercury lamp (Sankyo Denki G8T5) and 277-nm UVC LED
322 (Lextar PU35CM1) were used in this study. These UVC light sources were measured using a calibrated
323 spectroradiometer (GL Spectis 4.0) with an absolute measurement uncertainty of less than 6%. To provide
324 a comparative UVGI efficacy study between these UVC light sources, the radiant intensity of the far UVC
325 and mercury lamp is measured at different distances while the UVC LEDs are driven at different constant
326 drive currents to obtain a common UV intensity of 73 µW/cm^2. The UVC LED, with a beam angle of 120^o,
327 is assembled into a 5 x 5 array at a working distance of 12 cm to ensure uniform UV intensity across the
328 surface of the petri dish. The relative wavelength spectra of the light sources are shown in **Fig. S1**. Based
329 on the UV intensity readings, an enclosure is fabricated for each light source and the radiant intensity of
330 the enclosure is further validated with the spectroradiometer as shown in **Fig. S2**.

331 Viral infectivity experiments

332 The virus was propagated as previously described and stored in virus infection medium at 10^8 PFU/ml. For
333 each irradiation, 100 µl of virus suspension was placed on a 3-cm petri dish. After each irradiation, the virus
334 was subjected to serial dilution of 5 times, and 50 µl of each condition is diluted with 450 µl of virus infection

335 medium into 24-hour old and 80-90 % confluent MRC-5 or HCT-8 cells in 6-well plates. The cells were
336 incubated with the virus for 1 hour in a humidified incubator with 5% CO_2 before addition of a liquid overlay
337 medium, 3% carboxymethylcellulose, is applied to the cells to restrict virus growth to the originally infected
338 loci of cells. The cells are incubated at 37C in a 5% CO_2 incubator for 3 days before the liquid overlay
339 medium is aspirated and fixation with 4% paraformaldehyde is performed at room temperature for an hour.
340 Staining with 0.5% crystal violet is then conducted and the plaques are then quantified.

341 Immunofluorescence experiments

342 To assess whether 5 minutes of various UVC illumination reduces the number of infected cells,
343 immunostaining was performed to detect the presence of OC43 viral particles in the host human cells.
344 Briefly, 2 x 10^5 HCT-8 cells were plated in each petri dish one day before the experiment. The viral
345 suspension after their respective treatments was overlaid on the monolayer of host cells. After one hour of
346 incubation, the cells were washed with PBS and incubated for two days in fresh medium. The cells were
347 then fixed with 4% paraformaldehyde at room temperature for 15 minutes and washed with PBS before
348 being labelled with anti-Coronavirus OC43 Spike Protein antibody (CusaBio Technology LLC, Houston, TX,
349 USA) 1:500 in PBS containing 2 % bovine serum albumin (BSA) and 0.1 % TBS-T. Cells were then washed
350 with PBS and labelled with goat anti-rabbit Alexa Fluor-488 (Life Technologies, Grand Island, NY) in PBS
351 containing 2 % BSA at room temperature for an hour with gentle shaking. Following washing with PBS, the
352 cells were stained with DAPI and observed with the 40x objective of Nikon Ti-2 TIRF microscope.

353 Reverse Transcriptase Experiments

354 Beta-coronavirus RNA was extracted from the viral samples on each petri dish using the QiAmp Viral RNA
355 mini kit (Qiagen) following the manufacturer's instructions. 5 µl of each sample was used for qRT-PCR
356 analysis utilizing the TaqPath 1-step RT-qPCR master mix CG (Applied Biosystems) and the primer set
357 spanning a target region of 68bp for HCoV-OC43 as reported (20). The forward primer is 5'-
358 ATGTTAGGCCGATAATTGAGGACTAT-3 and the reverse primer is 5′-AATGTAAAGATGGCCGCGTATT-
359 3′. The analysis was then performed using the Quantstudio 5 software.

360 Protein degradation experiments

The antibodies that were utilized for western blots in this paper includes anti-Coronavirus OC43 Spike Protein antibody (CusaBio Technology LLC, Houston, TX, USA) and SARS-CoV-2 Spike RBD antibody (SinoBiological). All coronavirus purified spike proteins were obtained from SinoBiological. All samples for western blot were lysed in 2x Lamelli buffer and incubated in room temperature for 20 minutes before loading. Approximately 200 ng of protein sample is loaded for silver staining experiments and 1ug of protein sample is loaded for western blot experiments. The lysates were then subjected to SDS gel electrophoresis. For silver staining, we utilized the Pierce™ Silver Stain Kit (Thermofisher). For western blot, the samples were transferred to nitrocellulose membranes using iBlot2 (Life Technologies), blocked with 5% BSA in TBST and incubated with primary antibodies in 5% BSA. Membranes were then incubated with rabbit-IRDye 800 CW secondary antibodies and imaged on an Odyssey CLx (LI-COR). Absorption spectroscopy was performed on Nanodrop (Thermofisher).

Quantification and Statistical Analyses

The number of replicates (n) are indicated in the respective figure legends. For all statistical tests, significance was measured against $p < 0.05$. For comparisons of infectivity curves, 2-way analyses of variance (ANOVA) were carried out with the different UVC wavelengths and exposure time as the factors. All statistical analyses were performed with the GraphPad Prism Sotware 8.4.3 (GraphPad Software Inc., La Jolla, CA, USA) and all values are expressed as means +/- standard deviation.

Protein structure studies

The Desktop PyMOL 2.4 was used to visualize the protein structure of SARS-CoV-2 S glycoprotein (Protein Data Bank 6VXX) and calculate the distances between each indicated residue.